JOURNAL OF COMPUTATIONAL PHYSICS **124,** 254–270 (1996)
ARTICLE NO. 0058

A Chebyshev Pseudospectral Multidomain Method for a Boundary-Layer Problem

FRANCESCO MALARA

Dipartimento di Fisica, Università della Calabria, 87030 Cosenza, Italy

Received June 21, 1993; revised March 7, 1995

A multidomain pseudospectral method, which is based on Chebyshev polynomials expansions, is presented to solve an initial-boundary value problem in incompressible MHD, the tearing instability, in which a boundary layer is spontaneously generated inside the spatial domain. The method is based on a property of Chebyshev pseudospectral expansions which accurately describe functions having strong gradients localized near one of the Chebyshev domain boundaries. A comparison with the results of a single-domain pseudospectral method is performed, showing that, in the considered case, the multidomain technique furnishes a higher accuracy keeping the truncation error to a lower level. Because of the steeper Chebyshev spectra lower aliasing errors are obtained during the nonlinear stage of the instability.

1. INTRODUCTION

Pseudospectral methods represent a powerful tool in the numerical solution of nonlinear partial differential equations, and in particular, the fluid dynamics or the magnetohydrodynamics (MHD) equations. When the solutions are sufficiently regular, such methods give an accuracy which is generally higher than the accuracy of finite-difference methods which uses the same number of points in the spatial grid. For instance, when the solution is of $\mathscr{C}^\infty$-class spectral methods can be roughly considered as an infinite order (in space) numerical scheme.

Actually, the accuracy of spectral methods is strictly related to the regularity properties of the solution: when the quantities are of $\mathscr{C}^p$-class, spectral methods give origin to $(p+1)$-order schemes (see, e.g., [1]). As a consequence, a discontinuous solution is very poorly represented by a spectral method. This happens, for instance, in the inviscid fluid dynamics when a shock forms; the Gibbs phenomena generated by the discontinuity completely destroy the accuracy of the numerical solution. A way to overcome this problems is to use a multidomain technique; if the quantities are piecewise $\mathscr{C}^\infty$-class the spatial domain D can be divided into the union of K subdomains $D^{[\alpha]}$

$$D = \bigcup_{\alpha=1}^{K} D^{[\alpha]}.$$

We indicate by $\delta D^{[\alpha,\beta]} = D^{[\alpha]} \cap D^{[\beta]}$ the internal boundary between the αth and the βth subdomain. This partition must be such that any quantity remains of $\mathscr{C}^\infty$-class in each subdomain $D^{[\alpha]}$ during the time interval of interest. Then, a spectral method is used in each subdomain giving the appropriate boundary conditions at the internal boundaries. This kind of technique was used by Bonazzola and Marck [2] to describe the shock propagation in fluid dynamics; a moving internal boundary was placed at the shock location, at any time step; on this boundary the shock jump conditions were used as boundary conditions. This technique gives a very good approximation, since on each side of the shock the solution is of $\mathscr{C}^\infty$-class.

If diffusive phenomena are present, such as in the viscous fluid dynamics, the discontinuities associated with the shocks are smoothed out and are replaced by more or less narrow regions where the quantities of the problem vary with continuity from their values upstream to the values downstream. In such a case, in consequence of the regularity of the solution, a spectral method could be successfully used. However, in many applications the Reynolds number is quite large; this implies that the shock width is small and large gradients develop at the shock location; i.e., the shock tends to be a true discontinuity. In such a case, even though the quantities keep continuous, a large number of terms (harmonics) are necessary in their spectral representation in order to obtain a good accuracy in the numerical solution. If the number of harmonics is not sufficient to accurately describe fast variations in the solution, oscillations will appear at the shock location, similar to the Gibbs phenomena of the nonviscous case.

However, despite this analogy between the inviscid and the weakly viscous fluid dynamics, in the latter case a multidomain technique does not necessarily improve the accuracy of the numerical solution. Actually, when fast variation regions are present, instead of real discontinuities, a high spatial resolution is required in these regions. Then, the advantage of using a multidomain or a single-domain spectral technique depends only on the capability of this method to give such a high resolution in the "diffusivity" regions.

0021-9991/96 $18.00

This can be actually achieved if a Chebyshev pseudospectral method is employed in association with a multidomain technique. Solomonoff and Turkel [3] studied the properties of pseudospectral methods based on a Chebyshev expansion in cases when sharp variations are present in the solution. The standard pseudospectral Chebyshev expansion uses the following set of $(N + 1)$ collocation points

$$x_j = \cos\left(\frac{\pi j}{N}\right), \quad j = 0, ..., N, \tag{1}$$

in the spatial domain $D = [-1, 1]$; however, sets of collocation points different from (1) can also be used. In particular, Solomonoff and Turkel [3] considered both the standard collocation points (1) and a set of uniformly spaced collocation points. In both cases these authors found that the Chebyshev collocation methods give lower errors when sharp gradients or discontinuous derivatives occur near the boundaries of the spatial domain D than when they are near the center. This implies that a Chebyshev pseudospectral method can be advantageous in a multidomain technique to describe continuous solutions with localized sharp gradients, provided that these fast variation regions are near a boundary (internal or not) of some subdomain $D^{[\alpha]}$.

In this paper we consider a problem in which a boundary layer of small but finite amplitude is present, namely, the nonlinear development of the tearing instability in incompressible magnetohydrodynamics (MHD). In this problem a narrow region of strong localized gradients spontaneously forms around a well-determined plane surface (neutral sheet) inside the spatial domain. These gradients are directed perpendicular to the neutral sheet. Based on the results of Solomonoff and Turkel [3], one can expect that a substantial improvement of the spatial resolution can be achieved if an internal boundary between two subdomains is located at the neutral sheet, and Chebyshev expansions are carried out in both subdomains in the direction parallel to the gradients (i.e., perpendicular to the neutral sheet). In fact, in such a case the gradients turn out to be located close to the boundary of the Chebyshev meshes; this is the configuration in which a Chebyshev expansion gives the lowest errors [3].

In order to give a quantitative measure of the advantages of applying such a pseudospectral Chebyhev, multidomain technique to the solution of a boundary-layer problem we compared in details the results of this method with those obtained by a single domain technique. In the latter case, the boundary layer is located at the center of the spatial domain, i.e., far from the boundaries of the Chebyshev mesh. We show that the multidomain Chebyshev method gives a good accuracy with a number of Chebyshev polynomials much lower than the single-domain method. This, in turn, allows us to keep aliasing errors at a low level during the nonlinear stage of the instability.

2. THE NUMERICAL METHOD

The Chebyshev pseudospectral multidomain technique has been applied to the solution of an initial-boundary value problem for the incompressible magnetohydrodynamic equations. We considered two-dimensional configurations, where any physical quantity depends only on the X and Y variables, and only the X and Y components of vector quantities are nonvanishing. The equations of the incompressible MHD can be written in the dimensionless form

$$\frac{\partial Z_i^\sigma}{\partial t} + Z_k^{-\sigma}\frac{\partial Z_i^\sigma}{\partial x_k} + \frac{\partial P}{\partial x_i} = \chi\frac{\partial^2 Z_i^\sigma}{\partial x_k \partial x_k}, \quad i = 1, 2, \sigma = \pm, \tag{2}$$

$$\frac{\partial^2 P}{\partial x_k \partial x_k} = -\frac{\partial Z_k^+}{\partial x_m}\frac{\partial Z_m^-}{\partial x_k}, \tag{3}$$

where $\mathbf{Z}^\sigma$ and P are the dimensionless Elsasser variables and total pressure, respectively,

$$Z_i^\sigma = \frac{v_i}{c_A} + \sigma\frac{B_i}{B_0}, \quad i = 1, 2, \sigma = \pm; \quad P = \frac{p + B^2/8\pi}{\rho_0 c_A^2}.$$

In these equations $\mathbf{v}$ represents the velocity of the fluid, $\mathbf{B}$ is the magnetic field, p is the gas pressure, and $c_A = B_0/(4\pi\rho_0)^{1/2}$ is the Alfvén velocity, ρ_0 being the mass density which keeps constant and uniform, and B_0 a characteristic value for the magnetic field. The dimensionless space–time variables are $x_1 \equiv x = X/a$, $x_2 \equiv y = Y/a$, and $t = T(c_A/a)$, where a represents some characteristic length of the problem. Lower indices identify the vector cartesian components (e.g., $Z_1 \equiv Z_x$, $Z_2 \equiv Z_y$) and summation over the lower dummy indices is hereinafter understood. Finally, it has been assumed that $\nu = \eta c^2/(4\pi)$ (with ν the kinematic viscosity, η the resistivity, and c the velocity of the light) and the dissipation coefficient $\chi = \nu/(ac_A) = \eta c^2/(4\pi a c_A)$ has been defined. The space domain is given by the rectangle

$$D = \{(x, y) : x \in [-l, l], y \in [0, \pi R l]\},$$

where R is a parameter which determine the aspect ratio and l gives a measure of the domain width in normalized units.

The initial condition will be chosen in such a way that a boundary layer forms along the line $x = 0$. The location of this boundary layer does not change in time. Then, an enhanced spatial resolution is required close to the line

$x = 0$, where the largest gradients develop. This is achieved by dividing the spatial domain D in two subdomains, with the internal boundary located at the line $x = 0$. Pseudospectral Chebyshev expansions are carried out in both subdomains in the x-direction, i.e., parallel to such gradients. The results of this method will be compared with those obtained using a single-domain method. In this latter case, a single pseudospectral Chebyshev expansion is performed in the x-direction and the location of the boundary layer corresponds to the center of the Chebyshev mesh. It will be shown that the double-domain technique improves the accuracy of the numerical solution, in accordance with the results of Solomonoff and Turkel [3].

Concerning the boundary conditions, periodicity conditions are imposed on the boundaries $y = 0$ and $y = \pi Rl$, i.e., on those boundaries crossed by the boundary layer. The following free-slip conditions are imposed on the other pair of boundaries:

$$\begin{aligned} \frac{\partial Z_y^\sigma}{\partial x} &= 0, \quad \sigma = \pm, \text{ at } x = \pm l, t \geq 0, \\ \frac{\partial P}{\partial x} &= 0, \quad \text{at } x = -l, t \geq 0, \\ P &= P_0, \quad \text{at } x = l, t \geq 0, \end{aligned} \tag{4}$$

$t = 0$ being the initial time, along with the divergenceless conditions

$$\frac{\partial Z_x^\sigma}{\partial x} = -\frac{\partial Z_y^\sigma}{\partial y}, \quad \sigma = \pm, \text{ at } x = \pm l, t \geq 0. \tag{5}$$

If the divergence of $\mathbf{Z}^\sigma$ is vanishing at the initial time

$$\frac{\partial Z_k^\sigma}{\partial x_k} = 0, \quad \sigma = \pm \text{ for } (x, y) \in D \text{ at } t = 0, \tag{6}$$

Eqs. (2) and (3) with the boundary condition (5) ensure that the fields $\mathbf{Z}^\sigma$ remain divergenceless for any time $t \geq 0$.

The problem will be solved using both a double-domain technique and a single-domain technique. In the former case the domain D is divided in two subdomains (left and right) $D = D^{[L]} \cup D^{[R]}$, with $D^{[L]} = [-l, 0] \times [0, \pi Rl]$ and $D^{[R]} = [0, l] \times [0, \pi Rl]$; hereinafter we will indicate quantities relative to these two subdomains by the upper indices $^{[L]}$ and $^{[R]}$, respectively. Extra boundary conditions must be given on the internal boundary $x = 0$. In particular, we impose the following matching conditions:

$$Z_i^{\sigma[L]}(0, y, t) = Z_i^{\sigma[R]}(0, y, t), \quad y \in [0, \pi Rl], t \geq 0, i = 1, 2, \sigma = \pm, \tag{7a}$$

$$\frac{\partial Z_i^{\sigma[L]}}{\partial x}(0, y, t) = \frac{\partial Z_i^{\sigma[R]}}{\partial x}(0, y, t), \quad y \in [0, \pi Rl], t \geq 0, i = 1, 2, \sigma = \pm, \tag{7b}$$

$$P^{[L]}(0, y, t) = P^{[R]}(0, y, t), \quad y \in [0, \pi Rl], t \geq 0, \tag{7c}$$

$$\frac{\partial P^{[L]}}{\partial x}(0, y, t) = \frac{\partial P^{[R]}}{\partial x}(0, y, t), \quad y \in [0, \pi Rl], t \geq 0. \tag{7d}$$

These conditions will be discussed below, with regard to the regularity properties of the physical solution.

In the double-domain method, Eqs. (2) and (3) are numerically solved using a pseudospectral method in both $D^{[L]}$ and $D^{[R]}$; any quantity $f^{[\alpha]}(x, y, t)$ in the subdomain $D^{[\alpha]}$ at a given time t is approximated as a linear combination of a finite number of functions,

$$f^{[\alpha]}(x, y, t) = \sum_{m=0}^{M-1} \sum_{n=0}^{N} a_{nm}^{[\alpha]}(t)\, \phi_{nm}^{[\alpha]}(x, y), \tag{8}$$

where

$$\begin{aligned} \phi_{nm}^{[L]}(x, y) &= T_n(2x/l + 1)\, e^{2imy/(Rl)}, \quad (x, y) \in D^{[L]}, \\ \phi_{nm}^{[R]}(x, y) &= T_n(2x/l - 1)\, e^{2imy/(Rl)}, \quad (x, y) \in D^{[R]}, \end{aligned} \tag{9}$$

$T_n(\xi)$, $\xi \in [-1, 1]$, is the Chebyshev polynomial of degree n and i is the imaginary unity. The spatial grids of the collocation points used in the pseudospectral expansions are the sets

$$S^{[\alpha]} = \{(x_i^{[\alpha]}, y_j^{[\alpha]}), i = 0, ..., N, j = 0, ..., M - 1, \alpha = L, R\},$$

where

$$\begin{aligned} x_i^{[L]} &= l\,[-\cos(\pi i/N) - 1]/2, \\ x_i^{[R]} &= l\,[-\cos(\pi i/N) + 1]/2 \\ y_j^{[L]} &= y_j^{[R]} = \pi Rlj/M. \end{aligned} \tag{10}$$

These correspond to the standard collocation points used in the Fourier and Chebyshev pseudospectral expansions, respectively. We chose to use the standard collocation points because of the following reasons: Solomonoff and Turkel [3] considered the Chebyshev pseudospectral expansion of functions with large gradients near the boundaries and compared the accuracy when standard collocation points, or uniformly spaced points are respectively used. They found that the former choice is preferable, since in such a case lower absolute errors are obtained. Moreover, in the calculation of the expansion coefficients

with standard collocation points fast Fourier transform (FFT) algorithms can be employed; this transformation technique is faster than the matrix multiplication if the order N of the Chebyshev transform is sufficiently high (typically $N \gtrsim 100$) [5].

In the single-domain technique the pseudospectral expansion of a quantity $f(x, y, t)$ is

$$f(x, y, t) = \sum_{m=0}^{M-1} \sum_{n=0}^{2N} a_{nm}(t)\, \phi_{nm}(x, y), \tag{11}$$

where

$$\phi_{nm}(x, y) = T_n(x/l) e^{2imy/(Rl)}, \quad (x, y) \in D. \tag{12}$$

The spatial grid in this case is $S = \{(x_i, y_j),\ i = 0, ..., 2N,\ j = 0, ..., M - 1\}$, where

$$x_i = -l \cos[\pi i/(2N)], \quad y_j = \pi R l j/M. \tag{13}$$

The Chebyshev expansion is performed using $N + 1$ polynomials per each of the two subdomains in the double-domain case (see Eq. (8)), while $2N + 1$ polynomials are employed in the single-domain case (Eq. (11)). Then, the total number of polynomials in the two cases is almost the same and this fact makes clearer the comparison between the results obtained by the two different methods.

The time dependence in Eqs. (2) and (3) is treated by a second-order numerical scheme. In particular, a semi-implicit method is used [6, 7] in order to avoid the constraint of the Courant condition, which would become very severe in consequence of the high density of collocation points near the boundaries at $x = \pm l$ and $x = 0$ [8]. Given the solution $(\mathbf{Z}^{\sigma(n)}, P^{(n)})$ at the time $t_n = n\ \Delta t$ (Δt being the time step amplitude), the solution $(\mathbf{Z}^{\sigma(*)}, P^{(*)})$ at an intermediate time $t^* = t_n + \theta \Delta t$, $\frac{1}{2} < \theta \leq 1$, is first calculated using the equations

$$\frac{Z_i^{\sigma(*)} - Z_i^{\sigma(n)}}{\theta \Delta t} + Z_k^{-\sigma(n)} \frac{\partial Z_i^{\sigma(n)}}{\partial x_k} + \frac{\partial P^{(n)}}{\partial x_i} = \frac{\chi}{2} \frac{\partial^2}{\partial x_k \partial x_k} [Z_i^{\sigma(*)} + Z_i^{\sigma(n)}], \quad i = 1, 2,\ \sigma = \pm, \tag{14a}$$

$$\frac{\partial^2 P^{(*)}}{\partial x_k \partial x_k} = -\frac{\partial Z_k^{+(*)}}{\partial x_m} \frac{\partial Z_m^{-(*)}}{\partial x_k} \tag{14b}$$

and imposing the boundary conditions (4) and (5) and the matching conditions (7) to $Z_i^{\sigma(*)}$ and $P^{(*)}$. The upper index in parentheses identifies the time step. This solution is used to evaluate both the nonlinear term and the pressure gradient term in Eq. (2); then the solution at the time t_{n+1} is calculated using the equations

$$\frac{Z_i^{\sigma(n+1)} - Z_i^{\sigma(n)}}{\Delta t} + Z_k^{-\sigma(*)} \frac{\partial Z_i^{\sigma(*)}}{\partial x_k} + \frac{\partial P^{(*)}}{\partial x_i} - \Delta t c_k^2 \frac{\partial^2 Z_i^{\sigma(n+1)}}{\partial^2 x_k} = -\Delta t c_k^2 \frac{\partial^2 Z_i^{\sigma(n)}}{\partial^2 x_k} + \frac{\chi}{2} \frac{\partial^2}{\partial x_k \partial x_k} [Z_i^{\sigma(n+1)} + Z_i^{\sigma(n)}], \tag{15a}$$

$$i = 1, 2,\ \sigma = \pm;$$

$$\frac{\partial^2 P^{(n+1)}}{\partial x_k \partial x_k} = -\frac{\partial Z_k^{+(n+1)}}{\partial x_m} \frac{\partial Z_m^{-(n+1)}}{\partial x_k} \tag{15b}$$

and imposing the boundary conditions (4) and (5) and the matching conditions (7) to $Z_i^{\sigma(n+1)}$ and $P^{(n+1)}$.

The whole scheme (14)–(15) depends on the numerical parameters θ, c_1, and c_2, as well as on Δt. These parameters must be tuned in order to have a good accuracy and to avoid numerical instabilities. Both Eqs. (14) and (15) are implicit, because it is necessary to invert some differential operator in order to calculate $(\mathbf{Z}^{\sigma(*)}, P^{(*)})$ and $(\mathbf{Z}^{\sigma(n+1)}, P^{(n+1)})$, respectively.

Concerning the matching conditions (7), from the theory of the tearing instability [4] we know that in the physical problem the solution is continuous in the whole spatial domain up to the second-order space derivatives, although strong gradients form at the boundary layer. The matching conditions (7) applied to the time-discretized equations (14)–(15) ensure all the quantities, up to the second-order space derivatives, are continuous across the boundary $x = 0$ at each time step, provided that this condition is satisfied at the initial time. We show this point inductively; let us assume that $\mathbf{Z}^{\sigma(0)}$ and $P^{(0)}$ (at the initial time $t = 0$), as well as $\mathbf{Z}^{\sigma(n)}$ and $P^{(n)}$ (at a given time t_n), along with their x and y derivatives up to the second-order, are continuous across the internal boundary $x = 0$. The matching conditions (7) applied at the time t^* ensure that: (i) all the quantities are continuous across $x = 0$; (ii) their first-order x-derivatives are continuous across $x = 0$; (iii) in consequence of the point (i), their y-derivatives of any order are continuous across $x = 0$. Since, from Eqs. (14), the second order x-derivatives at $t = t^*$ are continuous functions of the above quantities, we conclude that $\mathbf{Z}^{\sigma(*)}$ and $P^{(*)}$ are continuous across the internal boundary up to the second-order derivatives. Using a similar argument on Eqs. (15) with the same matching conditions, it is shown that also $\mathbf{Z}^{\sigma(n+1)}$ and $P^{(n+1)}$ have these same regularity properties.

On the other hand, the regularity of the first- and second-order derivatives is necessary in order to ensure the continuity across $x = 0$ of the solutions. In fact, if, for instance, the derivative $\partial^2 Z_i^{(n)}/\partial x^2$ were discontinuous at $x = 0$, this would produce a discontinuity in $Z_i^{(n+1)}$ at the next time step. Moreover, the induction argument points out that the initial conditions of all the quantities must be chosen as at least $\mathscr{C}^2$-class functions on the whole space domain.

Finally, it is worth noting that the above regularity prop-

erties of the solutions are kept by the time scheme (14)–(15) because the scheme is implicit with respect to the second-order derivative terms. On the contrary, using an explicit time scheme, the continuity across the internal boundary of the second-order x-derivatives would not be ensured, and it should be explicitly added to the other matching conditions (7).

Equations (14) and (15) are transformed in the spectral space. Let us consider first the double-domain case. In the following we will indicate by $\hat{f}^{[\alpha]}(x, m)$ the mth coefficient of the Fourier expansion of a quantity $f^{[\alpha]}(x, y)$ at a given time:

$$f^{[\alpha]}(x, y) = \sum_{m=0}^{M-1} \hat{f}^{[\alpha]}(x, m)\, e^{2imy/(Rl)}.$$

Equations (14) and (15) are written in the Fourier space, for the subdomains $D^{[L]}$ and $D^{[R]}$ separately. All these equations can be set in the following general form, along with their boundary conditions,

$$\left.\begin{aligned} \left[\frac{d^2}{dx^2} - \kappa^2(m)\right] \hat{f}^{[\alpha]}(x, m) &= \hat{G}^{[\alpha]}(x, m) && \text{(16a)}\\ \ell^{[\alpha]}[\hat{f}^{[\alpha]}(x, m)] &= \hat{\beta}^{[\alpha]}(m) && \text{(16b)} \end{aligned}\right\}, \quad m = 0, ..., M-1, \alpha = L, R;$$

and the matching conditions,

$$\left.\begin{aligned} \hat{f}^{[L]}(0, m) &= \hat{f}^{[R]}(0, m) && \text{(17a)}\\ \frac{d\hat{f}^{[L]}}{dx}(0, m) &= \frac{d\hat{f}^{[R]}}{dx}(0, m) && \text{(17b)} \end{aligned}\right\}, \quad m = 0, ..., M-1;$$

where $\hat{f}^{[\alpha]}(x, m)$ indicates the Fourier coefficients of $Z_i^{[\alpha](*)}$, $Z_i^{[\alpha](n+1)}$, $P^{[\alpha](*)}$, or $P^{[\alpha](n+1)}$; $\hat{G}^{[\alpha]}(x, m)$ is the RHS, which depends on quantities relative to previous time steps; $l^{[L]}$ and $l^{[R]}$ are the linear operators which give the boundary conditions (4) and (5) in the Fourier space at the boundaries $x = -l$ and $x = l$, respectively; $\hat{\beta}^{[\alpha]}(m)$ are the corresponding RHS; $\kappa^2(m)$ are positive constants. Note that the solution of the problems (16)–(17) can be carried out independently for each Fourier harmonic; i.e., in the Fourier space we have to solve M decoupled problems.

For a given Fourier harmonic, the Eqs. (16a) can be considered as two distinct problems, each relative to one subdomain, which are coupled by the matching conditions (17a), (17b). These equations have been treated using an influence matrix method (see, e.g., Canuto *et al.* [9]) which allows us to decouple the two problems relative to each subdomain; we write the solutions $\hat{f}^{[\alpha]}(x, m)$ of the problem (16)–(17) in each subdomain as a linear combination of two functions,

$$\hat{f}^{[\alpha]}(x, m) = \hat{v}^{[\alpha]}(x, m) + \lambda_m\, \hat{w}^{[\alpha]}(x, m), \quad m = 0, ..., M-1, \alpha = L, R, \tag{18}$$

where λ_m is an appropriate constant which is defined by Eq. (21) and $\hat{v}^{[\alpha]}(x, m)$ and $\hat{w}^{[\alpha]}(x, m)$ are the guess and the correction solutions, respectively. The former is the solution of the problem

$$\left.\begin{aligned} \left[\frac{d^2}{dx^2} - \kappa^2(m)\right] \hat{v}^{[\alpha]}(x, m) &= \hat{G}^{[\alpha]}(x, m) && \text{(19a)}\\ l^{[\alpha]}[\hat{v}^{[\alpha]}(x, m)] &= \hat{\beta}^{[\alpha]}(m) && \text{(19b)}\\ \hat{v}^{[\alpha]}(0, m) &= \hat{\beta}_{\text{guess}}(m) && \text{(19c)} \end{aligned}\right\}, \quad m = 0, ..., M-1, \alpha = L, R,$$

where $\hat{\beta}_{\text{guess}}(m)$ represents a guess value for the solution $\hat{f}^{[\alpha]}(x, m)$ at the internal boundary $x = 0$. The solution $\hat{w}^{[\alpha]}(x, m)$ is determined by

$$\left.\begin{aligned} \left[\frac{d^2}{dx^2} - \kappa^2(m)\right] \hat{w}^{[\alpha]}(x, m) &= 0 && \text{(20a)}\\ l^{[\alpha]}[\hat{w}^{[\alpha]}(x, m)] &= 0 && \text{(20b)}\\ \hat{w}^{[\alpha]}(0, m) &= 1 && \text{(20c)} \end{aligned}\right\}, \quad m = 0, ..., M-1, \alpha = L, R.$$

The correction solution $\hat{w}^{[\alpha]}(x, m)$ does not depend on the time step, so it is calculated only once, at the beginning of the time advancing procedure, by solving the problems (20).

It can be easily verified that the linear combination (18) gives the solution of the problem (16)–(17), which is unique. In particular, the matching condition (17b) is satisfied by the following choice of the parameter λ_m:

$$\lambda_m = -\frac{\dfrac{d\hat{v}^{[R]}}{dx}(0, m) - \dfrac{d\hat{v}^{[L]}}{dx}(0, m)}{\dfrac{d\hat{w}^{[R]}}{dx}(0, m) - \dfrac{d\hat{w}^{[L]}}{dx}(0, m)}. \tag{21}$$

The guess solution $\hat{v}^{[\alpha]}(x, m)$ is continuous on the whole domain $\{x \in [-l, l]\}$, but its first derivative can be discontinuous at $x = 0$. The parameter λ_m is proportional to the jump in the first derivative of $\hat{v}^{[\alpha]}(x, m)$. This discontinuity is eliminated by adding the correction solution $\lambda_m \hat{w}^{[\alpha]}(x, m)$. Actually, the term $\lambda_m \hat{w}^{[\alpha]}(x, m)$ has also a disconti-

nuity in the first derivative at $x = 0$ which exactly smooths out the discontinuity of $d\hat{v}^{[\alpha]}(x, m)/dx$.

The guess solutions $\hat{v}^{[\alpha]}(x, m)$ depend on the quantities $\hat{\beta}_{\text{guess}}(m)$. These are free parameters which can in principle be chosen in an arbitrary way, since for any choice of $\hat{\beta}_{\text{guess}}(m) \equiv \hat{v}^{[\alpha]}(0, m)$ the corresponding guess solutions $\hat{v}^{[\alpha]}(x, m)$ can be corrected by adding the appropriate correction term $\lambda_m \hat{w}^{[\alpha]}(x, m)$. However, in order to avoid too large roundoff errors in the linear combination (18), the guess solutions $\hat{v}^{[\alpha]}(x, m)$ should not be too far from the final solutions $\hat{f}^{[\alpha]}(x, m)$. The amount of the correction can be evaluated defining the following quantities

$$\Delta\hat{f}^{[\alpha]}(m) \equiv \frac{\|\hat{f}^{[\alpha]}(x, m) - \hat{v}^{[\alpha]}(x, m)\|_\infty}{\|\hat{f}^{[\alpha]}(x, m)\|_\infty}, \tag{22}$$

where, as usual, $\|g(x)\|_\infty = \sup\{g(x), x \in [-l, l]\}$. In particular, we will require that

$$\Delta\hat{f}^{[\alpha]}(m) \ll 1, \quad m = 0, ..., M-1, \alpha = L, R. \tag{23}$$

In the Appendix it is shown that $\|\hat{w}^{[\alpha]}(x, m)\|_\infty = 1$; then, from Eq. (18) it follows that

$$\Delta\hat{f}^{[\alpha]}(m) = |\lambda_m|/\|\hat{f}^{[\alpha]}(x, m)\|_\infty; \tag{24}$$

i.e., the correction is proportional to $|\lambda_m|$. Evaluating Eq. (18) at $x = 0$ and taking into account that $\hat{w}^{[\alpha]}(0, m) = 1$, we find

$$\lambda_m = \hat{f}^{[\alpha]}(0, m) - \hat{v}^{[\alpha]}(0, m) = \hat{f}^{[\alpha]}(0, m) - \hat{\beta}_{\text{guess}}(m). \tag{25}$$

Thus, in order to have small values for the correction parameters $\Delta\hat{f}^{[\alpha]}(m)$ we have to choose the trial boundary condition $\hat{\beta}_{\text{guess}}(m)$ sufficiently close to $\hat{f}^{[\alpha]}(0, m)$. In particular, at any time step we used the boundary condition

$$\hat{\beta}_{\text{guess}} = \hat{f}^{[\alpha],(n-1)}(0, m), \tag{26}$$

where the RHS of Eq. (26) indicates the value of $\hat{f}^{[\alpha]}(0, m)$ at the previous time step. With this choice of the trial boundary condition the parameters λ_m are quantities of order Δt,

$$\lambda_m = \frac{\partial\hat{f}^{[\alpha]}}{\partial t}(0, m)\, \mu\, \Delta t + O(\Delta t^2),$$

where $\mu = \theta$ when the solution is calculated at the intermediate time t^* or $\mu = 1$ when the solution is calculated at the time t_{n+1}. The correction $\Delta\hat{f}^{[\alpha]}$ becomes, to the lowest order in Δt,

$$\Delta\hat{f}^{[\alpha]} \cong \Delta t/\tau_m, \tag{27}$$

where

$$\tau_m = \frac{\|\hat{f}^{[\alpha]}(x, m)\|_\infty}{|(\partial\hat{f}^{[\alpha]}/\partial t)\,(0, m)|}$$

represents a characteristic evolution time of the solution $\hat{f}^{[\alpha]}$ at $x = 0$. In conclusion, using the boundary condition (26), condition (23) is satisfied for sufficiently small values of Δt, namely,

$$\Delta t \ll \min\{\tau_m, m = 0, ..., M-1\}.$$

In the case of the single-domain technique, Eqs. (16)–(17) are replaced by the equations

$$\left[\frac{d^2}{dx^2} - \kappa^2(m)\right]\hat{f}(x, m) = \hat{G}(x, m) \tag{28a}$$

$$l^{[L]}[\hat{f}(x, m)] = \hat{\beta}^{[L]}(m), \quad m = 0, ..., M-1, \tag{28b}$$

$$l^{[R]}[\hat{f}(x, m)] = \hat{\beta}^{[R]}(m) \tag{28c}$$

which are solved by a Chebyshev pseudospectral technique, with the standard spatial mesh given by Eq. (13). The method is the same as that employed to solve the problem (19) or (20). Since in the single-domain case the order of the Chebyshev transforms is $2N$, the solution of Eqs. (28a), (28b), (28c) requires to solve a $(2N + 1) \times (2N + 1)$ linear system.

3. NUMERICAL RESULTS

The tearing instability represents the physical problem which will be used as a test for the numerical technique described in the previous section. Since the first work by Furth *et al.* [4], the tearing instability has received a lot of attention in plasma physics research. It develops in a magnetofluid for configurations in which some component of the magnetic field vanishes on a given surface (neutral surface). A small but finite value of the resistivity η is also required, in order to allow changes in the magnetic lines topology. In particular, we will consider the case of a plane sheet pinch, where the equilibrium configuration is given by a vanishing velocity $\mathbf{v}_{\text{eq}} = 0$ and the magnetic field

$$\mathbf{B}_{\text{eq}} = B_0\left[\text{tgh}\left(\frac{X}{a}\right) + b\left(\frac{X}{a}\right)\right]\mathbf{e}_y, \tag{29}$$

where B_0 gives the magnitude of the magnetic field, a is the shear length, $\mathbf{e}_y$ is the unity vector along the Y-direction of a cartesian frame of reference, and b is a constant. The second term in the expression (29) allows $\mathbf{B}_{eq}$ to satisfy the boundary condition (4). For this equilibrium structure the neutral surface is represented by the plane $X = 0$. At this location a boundary layer develops in consequence of the tearing instability. In this layer the velocity and the magnetic field are continuous but they present sharp gradients in the direction of the X-axis, i.e., perpendicularly to the neutral surface. During the growth of the unstable modes, these gradients remain localized near the neutral surface of the equilibrium structure. The thickness of the boundary layer depends on the resistivity η, in that it is smaller for lower values of η.

Because of these features, a multidomain technique with Chebyshev expansions is well suited to give an accurate numerical solution of this problem. In this section we present the results of some simulations of the tearing instability. In particular, the results obtained using the double-domain Chebyshev technique will be compared with those obtained using the single-domain technique. In order to excite the instability, at the initial time $t = 0$ a small amplitude random perturbation is superposed on the equilibrium magnetic field $\mathbf{B}_{eq}$ (Eq. (29)). In particular, the initial condition has the form

$$\mathbf{Z}^{\sigma}(x, y, t_0) = \mathbf{Z}^{\sigma}_{eq}(x) + \mathbf{Z}^{\sigma}_{pert}(x, y), \sigma = \pm, \tag{30}$$

where

$$\begin{aligned}\mathbf{Z}^{\sigma}_{eq}(x) &= \sigma\, \mathbf{B}_{eq}(x)\\ \mathbf{Z}^{\sigma}_{pert}(x, y) &= \mathrm{curl}\,\{[\phi^{\sigma}_{R,pert}(x)\cos(2y/Rl)\\ &\quad - \phi^{\sigma}_{I,pert}(x)\sin(2y/Rl)]\,\mathbf{e}z\}\end{aligned}$$

and $\mathbf{e}_z$ is the vector unity perpendicular to the simulation plane and $\phi^{\sigma}_{R,pert}(x)$ and $\phi^{\sigma}_{I,pert}(x)$ represent the initial small amplitude perturbation of the vector potential. The initial condition (30) corresponds to the excitation of the $m = 0$ and $m = 1$ Fourier harmonics of $\mathbf{Z}^{\sigma}$. Moreover, the form (30) ensures that the initial condition is divergenceless.

The functions $\phi^{\sigma}_{R,pert}(x)$ and $\phi^{\sigma}_{I,pert}(x)$ must be chosen so as to satisfy the boundary conditions (4); i.e., we required that

$$\frac{d^2\,\phi^{\sigma}_{R,pert}}{dx^2} = 0, \quad \frac{d^2\,\phi^{\sigma}_{I,pert}}{dx^2} = 0 \tag{31}$$

at the boundaries $x = \pm l$. Moreover, when the double-domain Chebyshev technique is used the matching conditions (7a)–(7d) are to be satisfied, which implies the continuity of

$$\phi^{\sigma}_{R,pert}(x), \frac{d\,\phi^{\sigma}_{R,pert}}{dx}(x), \frac{d^2\,\phi^{\sigma}_{R,pert}}{dx^2}(x), \frac{d^3\,\phi^{\sigma}_{R,pert}}{dx^3}(x) \quad \text{at } x = 0, \tag{32}$$

the continuity of

$$\phi^{\sigma}_{I,pert}(x), \frac{d\,\phi^{\sigma}_{I,pert}}{dx}(x), \frac{d^2\,\phi^{\sigma}_{I,pert}}{dx^2}(x), \frac{d^3\,\phi^{\sigma}_{I,pert}}{dx^3}(x) \quad \text{at } x = 0. \tag{33}$$

The functions $\phi^{\sigma}_{R,pert}(x)$ and $\phi^{\sigma}_{I,pert}(x)$ have been determined, giving their Chebyshev expansions. The conditions (31)–(33) represent constraints which must be fulfilled by such expansions; they have been used to determine a number of Chebyshev coefficients as functions of the remaining ones. The latter have been chosen so to obtain exponentially decaying spectra. This technique allowed us to build up an initial condition which is very smooth and, at the same time, which satisfies all the boundary and matching conditions.

The amplitude of the initial perturbation has been chosen so that the perturbation energy to the equilibrium structure energy ratio is a small quantity. In particular, indicating such a ratio by

$$\varepsilon = \frac{1}{4E_0}\int_D [\mathbf{Z}^{+^2}_{pert}(x, y) + \mathbf{Z}^{-^2}_{pert}(x, y)]\,dx\,dy,$$

where

$$\mathbf{E}_0 = \frac{1}{4}\int_D [\mathbf{Z}^{+^2}_{eq}(x, y) + \mathbf{Z}^{-^2}_{eq}(x, y)]\,dx\,dy \tag{34}$$

is the equilibrium structure initial energy, we chose the perturbation amplitude such that $\varepsilon = 10^{-7}$, i.e., much less than the equilibrium magnetic field amplitude.

The values of the parameters used in the runs are: $\chi^{-1} = 2 \times 10^3$, $R = \frac{8}{3}$, $l = 10$. With this choice the Fourier harmonic $m = 1$ turns out to be comprised in the unstable wavelengths range, close to the most unstable wavelength [10–12]. Moreover, the spatial domain width ($2l$ in our units) is much larger than the width of the equilibrium magnetic field shear (equal to 1 in our units); then, the boundary condition at $x = \pm l$ do not sensibly affect the evolution of the instability.

In order to study the capability of the pseudospectral Chebyshev expansion to describe the formation of the boundary layer, different runs have been performed using a different number of Chebyshev polynomials. In particular, we considered the cases $N = 32$, $N = 64$, and $N = 128$, corresponding respectively to 33 + 33, 65 + 65, and

129 + 129 Chebyshev polynomials in the double-domain case (see Eq. (8)), and to 65, 129, and 257 Chebyshev polynomials in the single domain case (see Eq. (11)). Although only the $m = 0$ and $m = 1$ Fourier harmonics have been initially excited, nonlinear couplings transfer energy to higher wavenumbers. However, these couplings are rather weak because of the low energy level in the perturbation. So the Fourier spectrum of the solution is very steep and a small number of Fourier harmonics can be used. In particular, in all the runs we used $M = 32$ collocation points in the Fourier grid. The values of the other numerical parameters are $\Delta t = 4$, $\theta = 0.505$, $c_1 = 0.025$, $c_2 = 1$. We verified that with these values the scheme is numerically stable, in accordance with the results by Harned and Schnack [7].

Starting from the above smooth initial condition, for increasing time the $m = 1$ harmonic evolves giving origin to the unstable eigenmode which corresponds to that wavelength and to the given boundary conditions. In Figs. 1a and 1b the normalized kinetic energy $E_1^{\text{kin}}(t)$ of the $m = 1$ Fourier harmonic is plotted versus time, the normalized kinetic energy of the mth Fourier harmonic being defined as

$$E_m^{\text{kin}}(t) = \frac{1}{8E_0}\int_{-l}^{l} |\hat{\mathbf{Z}}^+(x, m, t) + \hat{\mathbf{Z}}^-(x, m, t)|^2 \, dx. \quad (35)$$

The time evolution of the normalized kinetic energy $E_1^{\text{kin}}(t)$ is plotted both in the double-domain (Fig. 1a) and in the single-domain (Fig. 1b) case, using different numbers of Chebyshev polynomials in the spectral expansions of the quantities.

The main features of the time evolution can be summarized as follows; during about the first 600 time units the kinetic energy grows in time, but relevant oscillations are superposed on this trend. These oscillations are gradually damped. This stage corresponds to the formation of the unstable eigenmode, which is characterized by strong gradients in the x-direction, localized around the line $x = 0$. From the time $t \approx 600$ on, the kinetic energy of the $m = 1$ harmonic grows exponentially up to the time $t \approx 1000$. This stage corresponds to the exponential growth of the unstable eigenmode, predicted by the linear theory of the tearing instability [4].

In the double-domain case (Fig. 1a) the plots corresponding to 33 + 33, 65 + 65, and 129 + 129 Chebyshev polynomials are, in practice, superposed. Then, if the double-domain Chebyshev technique is used, the evolution of the kinetic energy in the perturbation is well described also when a relatively low number of Chebyshev polynomials is employed, namely a total number of 66 polynomial in the whole domain.

A different behavior is observed when the single-domain technique is used (Fig. 1b). In particular, the time evolution is still well described with 129 and 257 Chebyshev polynomials, but this is not the case when spectral expansions with 65 polynomials are used. Actually, in this latter case the exponential growth of the kinetic energy appears to be sensibly slower than in all the other cases. In order to give a quantitative measure, we considered the time interval $600 \le t \le 1000$, corresponding to the exponential growth stage. During this time interval the behavior of the kinetic energy $E_1^{\text{kin}}(t)$ can be approximated by an exponential function

$$E_1^{\text{kin}}(t) \cong E\, e^{\gamma t} \quad (36)$$

with E and γ constant. The value of the growth rate γ has been determined fitting a linear function of the time on $\ln[E_1^{\text{kin}}(t)]$. We obtained $\gamma \cong 3.41 \times 10^{-3}$ in the single-domain case with 65 Chebyshev polynomials, while $\gamma \cong 4.23 \times 10^{-3}$ in all the other cases. This indicates that 65 polynomials in the single-domain case are not sufficient to accurately describe the time evolution of the energy in the perturbation.

The profiles of the real part of the $m = 1$ Fourier harmonic of the velocity and of the magnetic field, as functions of the x-variable, are shown in Figs. 2 and 3 at the time $t = 1000$, i.e., during the exponential growth stage. It can be seen that the solution has strong space variations around $x = 0$, as predicted by the linear theory [4, 10, 11]. The solutions obtained using the double-domain Chebyshev technique (Fig. 2) with 33 + 33, 65 + 65, and 129 + 129 Chebyshev polynomials are very close to one another, so to appear superposed. Only the x-component of the velocity perturbation (Fig. 2a) calculated with 33 + 33 polynomials presents some difference near the boundaries with respect to the profiles calculated using a higher number of polynomials. On the contrary, the boundary layer is well described also using 33 + 33 polynomials. Then, the resolution which is obtained using 66 polynomials with the double-domain technique is sufficient to describe the structure of the boundary layer associated with the tearing instability.

The corresponding profiles obtained using the single-domain technique are similar to those of the double-domain case, but not exactly the same. Actually, since the initial condition is different from that used in the double-domain case, the excited eigenmode has a different phase along the periodicity (y) direction, so the profiles of the real (and imaginary) part have a different amplitude with respect to the double domain case. Considering the Figs. 3 it is seen that the profiles obtained using 129 or 257 Chebyshev polynomials are superposed. On the contrary, the solution is sensibly different when 65 polynomials are employed: the amplitude of the perturbation is lower, in accordance with the results shown in Fig. 1b. Moreover, relevant short-scale oscillations are present in the y-compo-

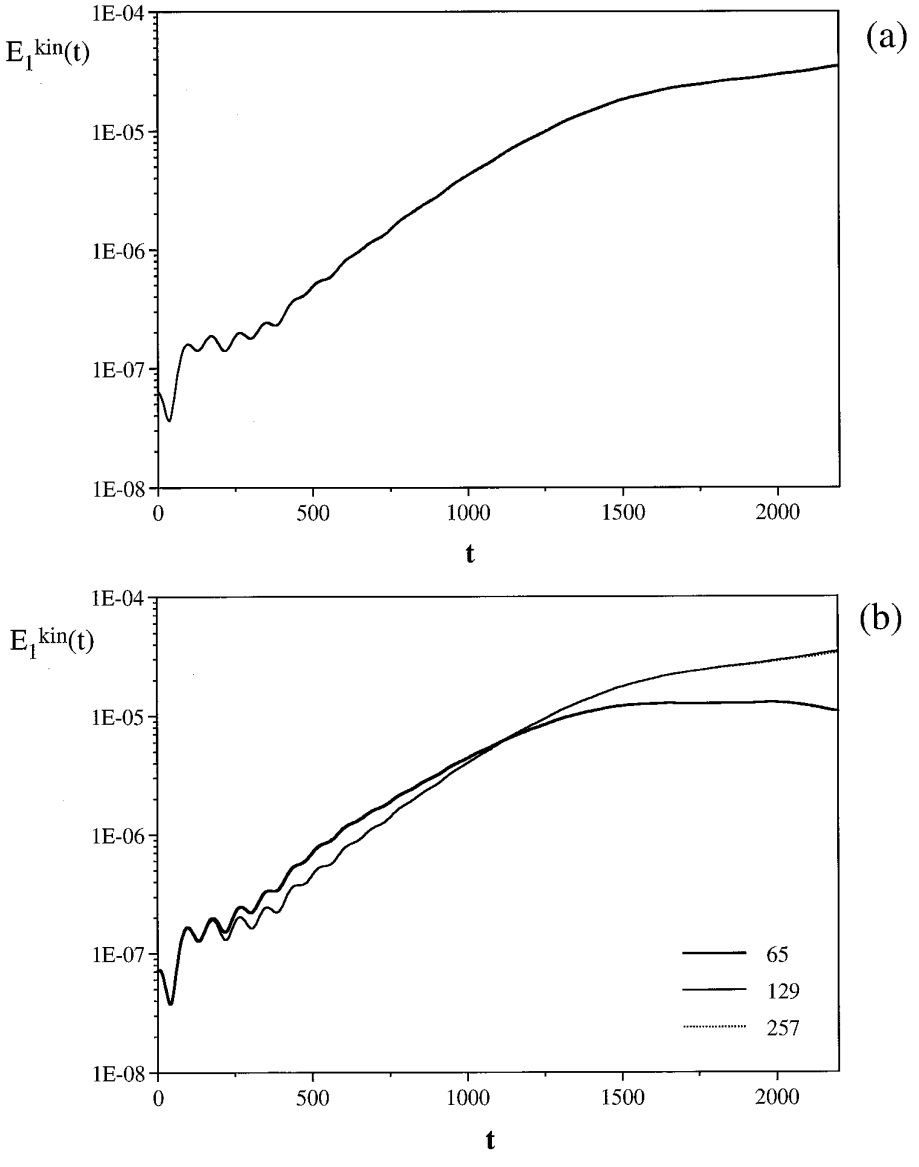

FIG. 1. The kinetic energy associated to the $m = 1$ Fourier harmonic, as a function of the time. Using the double domain technique the plots corresponding to 33 + 33, 65 + 65, and 129 + 129 Chebyshev polynomials are superposed (a). Using the single domain technique, this holds when 129 or 257 polynomials are used, while a different behavior is found with 65 polynomials (b).

nent velocity perturbation profile (Fig. 3b); the amplitude of such oscillations increases with the time. This phenomenon indicates that when 65 polynomials are used the Chebyshev expansion is unable to correctly describe the strong gradients which forms around $x = 0$.

In order to obtain further information on the accuracy of the solution we calculated the Chebyshev spectrum of the excited unstable eigenmode, which contains the boundary layer. This eigenmode corresponds to the $m = 1$ Fourier harmonic of $\mathbf{Z}^\sigma$. Since this quantity grows in time during the development of the instability, it has been normalized using its L^2-norm. Then, we define the mode $z_i^\sigma(x, t)$ by

$$z_i^\sigma(x,t) = \frac{\hat{Z}_i^\sigma(x,1,t)}{\left[\int_{-l}^{l} |\hat{Z}_i^\sigma(x',1,t)|^2\, dx'\right]^{1/2}} \tag{37}$$

which approximates the unstable eigenmode. The Chebyshev spectrum $z_{i,n}^\sigma(t)$ of the mode $z_i^\sigma(x, t)$ is defined by

$$z_i^\sigma(x,t) = \sum_{n=0}^{N} z_{i,n}^\sigma(t)\, T_n(x/l), \quad x \in [-l, l], i = x, y, \sigma = \pm, \tag{38}$$

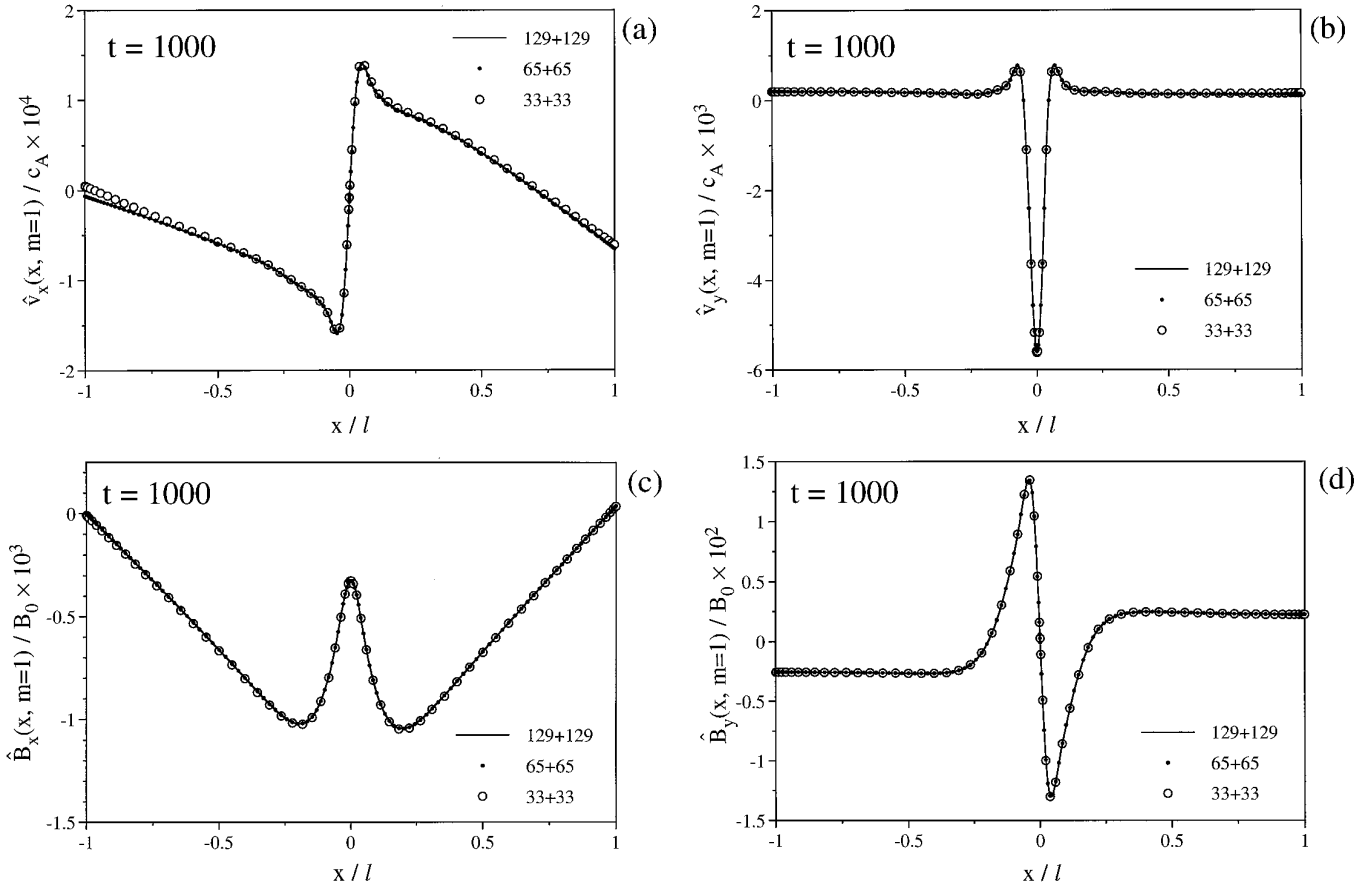

FIG. 2. The profiles, as functions of x, of the real part of the $m = 1$ Fourier harmonic of the velocity x-component (a) and y-component (b) and of the magnetic field x-component (c) and y-component (d) at the time $t = 1000$, obtained using the double-domain technique with 33 + 33, 65 + 65, and 129 + 129 Chebyshev polynomials.

in the single-domain case. In the double domain case we represent only the Chebyshev spectra relative to the right subdomain $D^{[R]}$; those relative to the left subdomain $D^{[L]}$ are very similar in consequence of the symmetry properties of the unstable eigenmode [4, 11]. In this case we define the spectrum $z^{\sigma}_{i,n}(t)$ by the relation

$$z^{\sigma}_i(x,t) = \sum_{n=0}^{N} z^{\sigma}_{i,n}(t)\, T_n(2x/l - 1), \qquad x \in [0,l],\ i = x, y,\ \sigma = \pm, \tag{39}$$

where

$$z^{\sigma}_i(x,t) = \frac{\hat{Z}^{\sigma}_i(x,1,t)}{\left[\int_0^l |\hat{Z}^{\sigma}_i(x',1,t)|^2\, dx'\right]^{1/2}}, \quad x \in [0,l].$$

In Figs. 4a and 4b the spectrum $|z^{+}_{x,n}(t)|$ is plotted for $t = 1000$ and $t = 2000$, respectively, in the double-domain case, using different values of N. The same quantity is plotted in Figs. 5a and 5b, in the single-domain case. The time $t = 1000$ approximately corresponds to the end of the exponential growth stage, while $t = 2000$ is during the instability saturation (see Figs. 1). Comparing the results shown in Figs. 4 and 5 it is seen that the Chebyshev spectra $|z^{+}_{x,n}(t)|$, obtained using the double-domain technique are much steeper than those obtained by the single-domain technique. Then, using the double-domain technique a small number of Chebyshev polynomials is required to represent the solution with a boundary layer at $x = 0$. On the contrary, using the single-domain technique the contribution of high-order Chebyshev polynomials in the spectral expansion of the boundary layer solution is much more relevant.

In consequence of this, representing the solution with the same number of Chebyshev polynomials, much lower truncation errors are obtained using the double-domain than the single-domain technique. An order of magnitude evaluation of the truncation error in the mode $z^{\sigma}_i(x,t)$ can be obtained in the following way. Let us consider first the

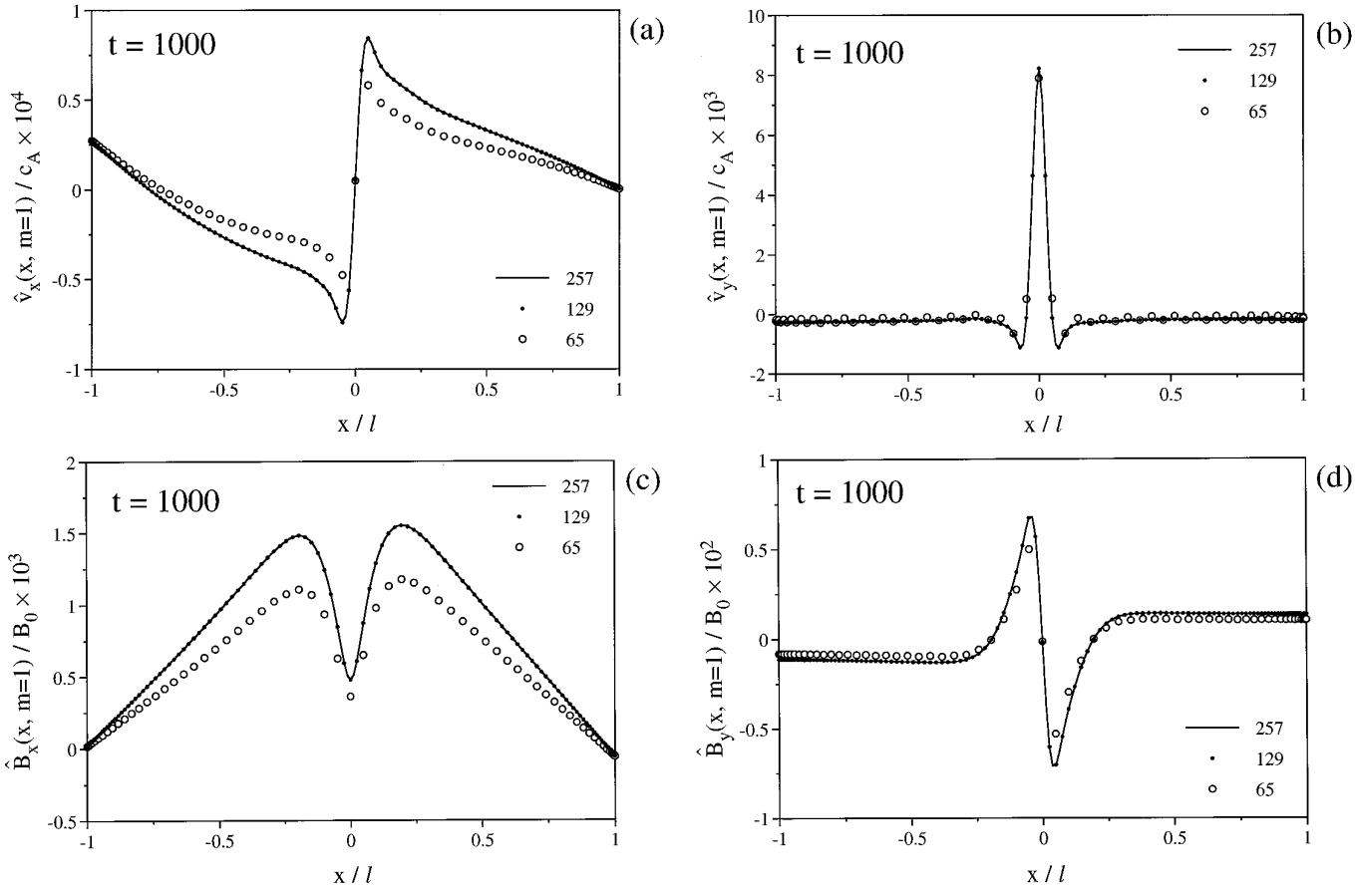

FIG. 3. The same profiles as those of Fig. 2, obtained using the single-domain technique with 65, 129, and 257 Chebyshev polynomials.

double-domain case. We indicate by $\tilde{z}_i^\sigma(x, t)$ the representation of the mode $z_i^\sigma(x, t)$ obtained using an infinite number of Chebyshev polynomials. Its spectral expansion is indicated by

$$\tilde{z}_i^\sigma(x, t) = \sum_{n=0}^{\infty} \tilde{z}_{i,n}^\sigma(t)\, T_n\left(\frac{2x}{l} - 1\right). \tag{40}$$

The sequence $\{|\tilde{z}_{i,n}^\sigma(t)|, n = 0, 1, ...\}$ goes to zero with a rate which depends on the regularity properties of $\tilde{z}_i^\sigma(x, t)$. If, for instance, $\tilde{z}_i^\sigma(x, t)$ is of C^{2p}-class with respect to the x-variable, then the inequality $|\tilde{z}_{i,n}^\sigma(t)| < 1/n^{2p}$ holds for sufficiently large n, for any time t [1]. This ensures that the series

$$\sum_{n=0}^{\infty} |\tilde{z}_{i,n}^\sigma(t)|$$

converges to a finite value. We define the truncation error at the Nth term, in the mode $z_i^\sigma(x, t)$ by

$$\delta_N z_i^\sigma(t) = \|z_i^\sigma(x, t) - \tilde{z}_i^\sigma(x, t)\|_\infty. \tag{41}$$

Looking at the spectra shown in Figs. 4a and 4b, it can be seen that the value of $|z_{i,n}^\sigma(t)|$ for a given n does not undergo important changes when the order N of the Chebyshev expansion is increased. This holds also for the complex coefficients $z_{i,n}^\sigma(t)$. Then, we can assume that

$$z_{i,n}^\sigma(t) \cong \tilde{z}_{i,n}^\sigma(t), \quad n = 0, ..., N. \tag{42}$$

The truncation error is then given by

$$\delta_N z_i^\sigma(t) \cong \left\| \sum_{n=N+1}^{\infty} \tilde{z}_{i,n}^\sigma(t)\, T_n\left(\frac{2x}{l} - 1\right) \right\|_\infty \tag{43}$$

$$\leq \sum_{n=N+1}^{\infty} |\tilde{z}_{i,n}^\sigma(t)|,$$

where we used the relation $\|T_n(x)\|_\infty = 1$, $n = 0, 1, ...$ The sum in the RHS of the inequality (43) gives an upper bound of the truncation error. In our runs we considered the cases with $N = 32$, $N = 64$, and $N = 128$. Since the sequence $\{|\tilde{z}_{i,n}^\sigma(t)|, n = 0, 1, ...\}$ goes to zero very rapidly with increas-

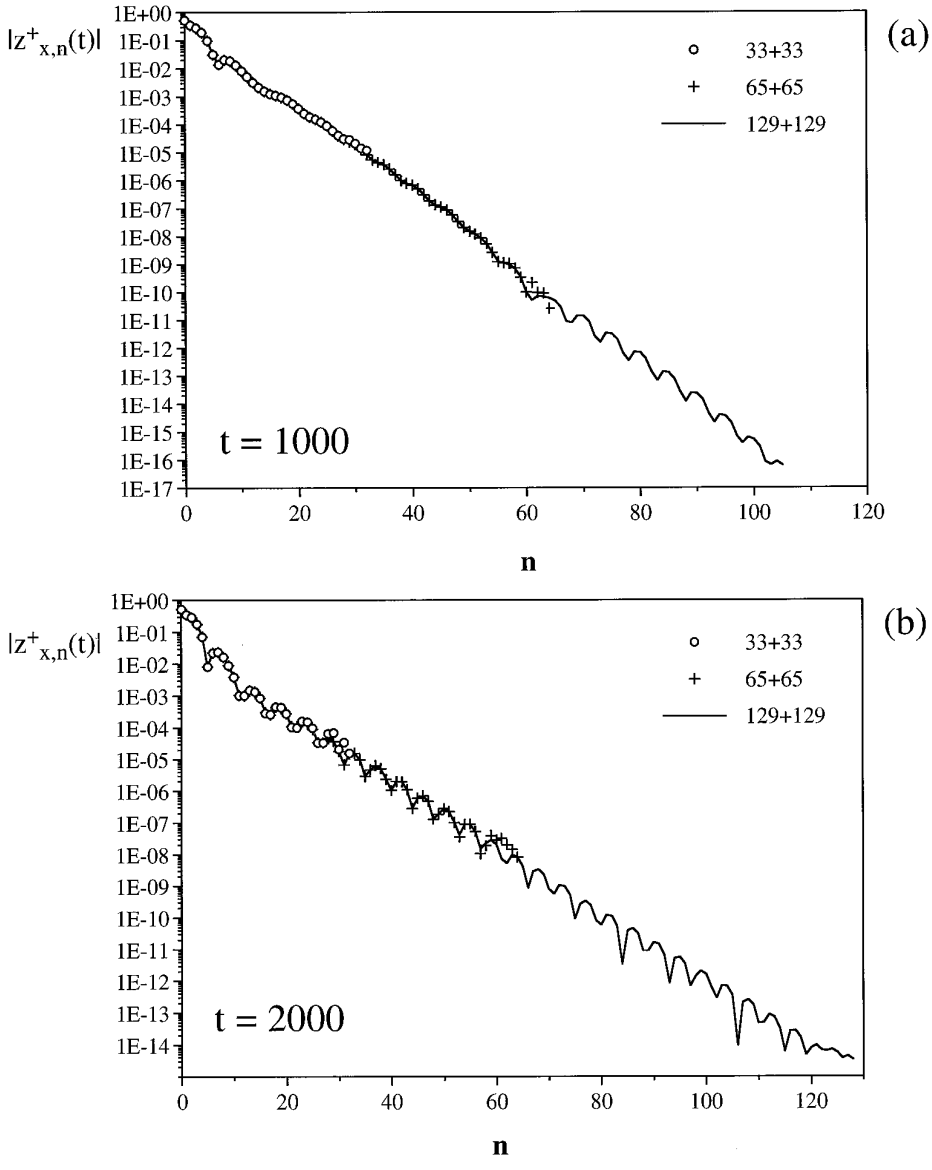

FIG. 4. The spectrum $|z^+_{x,n}(t)|$ of the normalized mode $z^+_x(x, t)$ plotted as a function of n at the time $t = 1000$ (a) and $t = 2000$ (b), using 33 + 33, 65 + 65, and 129 + 129 Chebyshev polynomials with the double-domain technique.

ing n (Figs. 4a and 4b), in the cases $N = 32$ and $N = 64$ a good estimation of the series at the RHS of (43) can be obtained, truncating such a series at the term corresponding to $n = 128$,

$$\delta_N z_i^\sigma(t) \leq \sum_{n=N+1}^{128} |\tilde{z}^\sigma_{i,n}(t)| \cong \Delta_N z_i^\sigma(t) \quad \text{with } N = 32 \text{ or } N = 64, \tag{44}$$

where

$$\Delta_N z_i^\sigma(t) = \sum_{n=N+1}^{128} |z^\sigma_{i,n}(t)|, \tag{45}$$

the terms of the sum (45) are those obtained by the numerical procedure using Chebyshev expansions with $N = 128$. The quantity $\Delta_N z_i^\sigma(t)$ represents an estimation of an upper bound for the truncation error of the mode $z_i^\sigma(x, t)$ in the cases in which the double-domain technique has been used with 33 + 33 or 65 + 65 polynomials. This quantity is plotted in Fig. 6 as a function of the time, relative to the component $z_x^+(x, t)$. For instance, at the time $t = 1000$ the truncation error of the mode $z_x^+(x, t)$ is less than 3×10^{-5} when 33 + 33 polynomials are used, while it is less than 2×10^{-10} using 65 + 65 polynomials. These values are actually small because the truncation error is evaluated for the normalized solution (see Eq. (37)), i.e., for a quantity whose L^2-norm is equal to 1. For increasing time the trun-

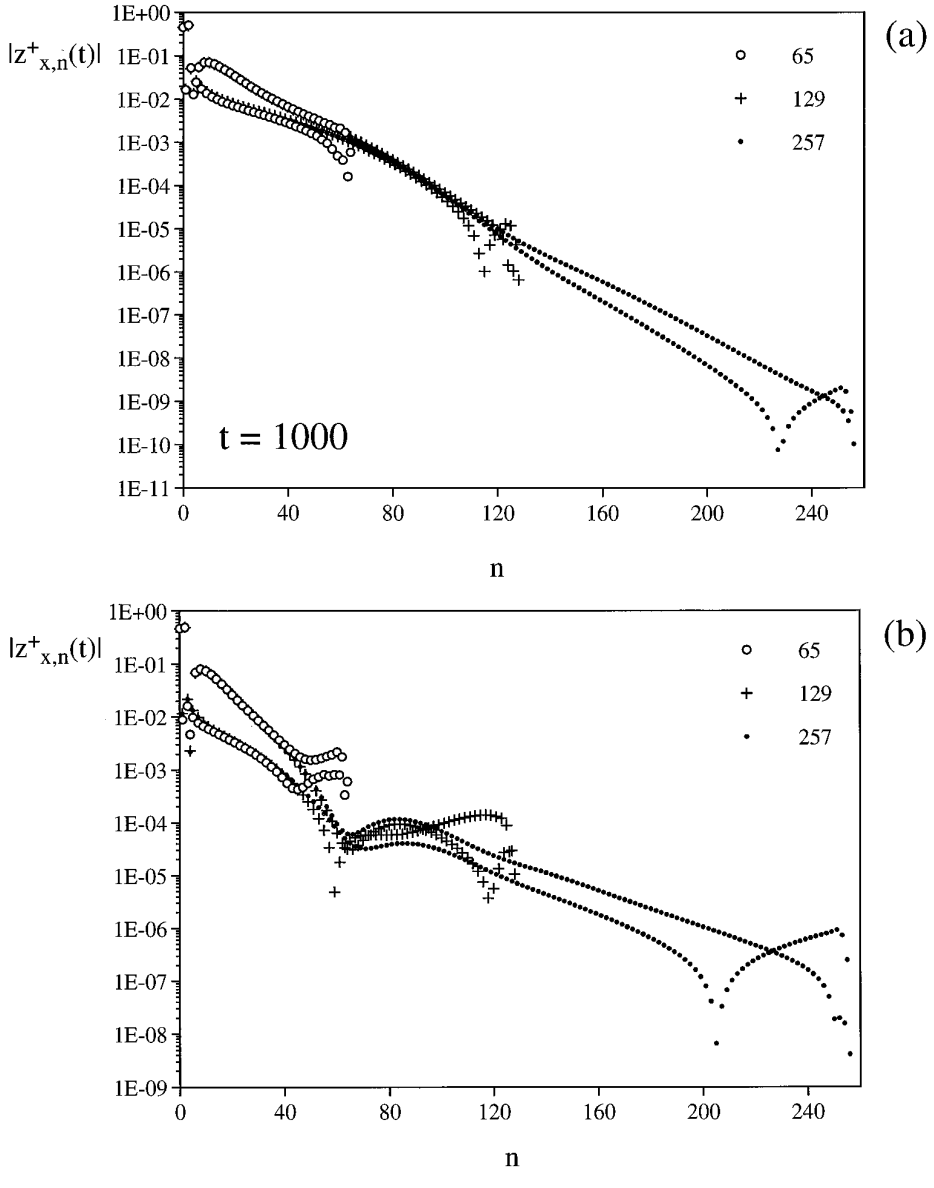

FIG. 5. The same as in Fig. 4, using 65, 129, and 257 Chebyshev polynomials with the single-domain technique.

cation error $\Delta_N z_x^+(t)$ increases in consequence of nonlinear effects which transfer energy towards the higher-order coefficients of the spectral expansion.

A similar procedure could be used to estimate the truncation error for the single-domain runs. Indeed, from Figs. 5a and 5b it can be seen that, although at $t = 1000$ the relation (42) is still relatively well satisfied (at least as an order of magnitude estimation), this is no more true at $t = 2000$. In fact, Fig. 5b shows that the high-n part of the spectrum strongly changes when increasing the order of the Chebyshev transform. Then, in the single-domain runs we can assume as an upper limit for the truncation error the quantity

$$\Delta_N z_i^\sigma(t) = \sum_{n=N+1}^{256} |z_{i,n}^\sigma(t)| \quad \text{with } N = 64 \text{ or } N = 128, \qquad (46)$$

but only during the first part of the runs, say for $t \leq 1000$. This quantity is also plotted on Fig. 6 (thick lines). Comparing with the results obtained with the double-domain Chebyshev technique, it can be seen that in this latter case the truncation error is orders of magnitude smaller than that obtained using the single-domain technique with the same number of Chebyshev polynomials.

This result is due to the fact that the strongest gradients in the solution are localized around the $x = 0$, which corresponds to the internal boundary of the double-domain

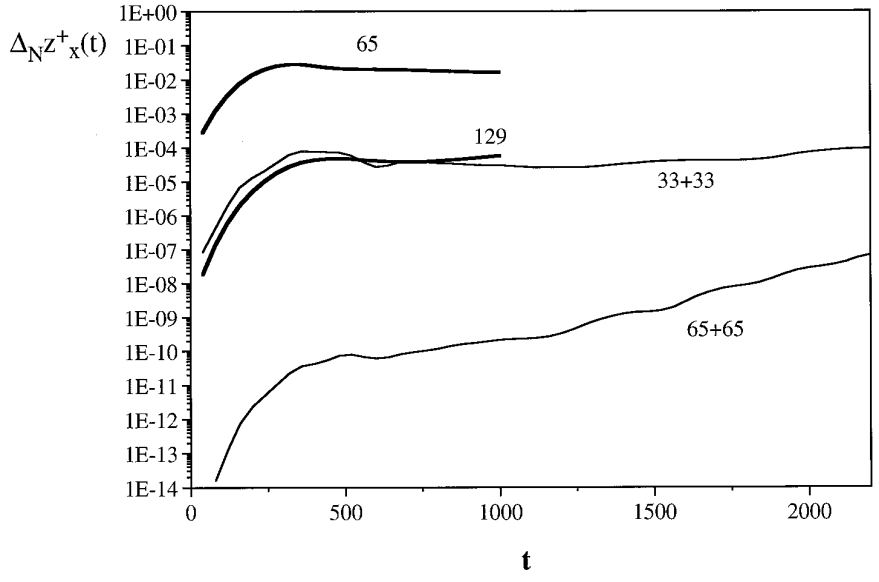

FIG. 6. The truncation error of the normalized mode x-component is plotted as a function of the time. The total number of the employed Chebyshev polynomials is indicated. Thick lines refer to single-domain runs while thin lines refer to double-domain runs.

case. Then, the accuracy of the Chebyshev expansion is much higher in this case, in accordance with the results of Solomonoff and Turkel [3].

The pseudospectral method used to calculate the nonlinear (products) terms in Eqs. (14) leads to aliasing errors [1, 13, 14]. These errors are more relevant during the last part of the runs, when nonlinear effects play an important role in the instability saturation. Such errors are smaller if the spectra of the quantities which are multiplied are steeper; i.e., the aliasing errors are smaller when the truncation errors are smaller. This implies that lower aliasing errors should be obtained with the double-domain technique.

The effects of aliasing errors in the single-domain runs can be observed in Figs. 5a and 5b; indeed, as already observed, the high-n part of the spectrum changes when the order of the Chebyshev polynomials is increased. This effect becomes more relevant with increasing time; actually, the amplitude of the perturbation grows in time, so the nonlinearities in the evolution equations (14) become more important. The same effect is much less relevant in the double-domain case (see Figs. 4a and 4b), even for $t = 2000$. Then, the small truncation errors obtained with the double-domain technique allow us to keep the aliasing errors to a lower level; this is useful in particular during the nonlinear stage of the instability.

A more quantitative evaluation of the effects of the truncation errors can be obtained, considering the divergence of the fields $\mathbf{Z}^\sigma$. The time evolution equations (2)–(3) ensure that $\partial Z_i^\sigma/\partial x_i = 0$ for $t > 0$, provided that: (i) the initial condition is divergenceless and (ii) $\partial Z_i^\sigma/\partial x_i$ is kept vanishing at the boundaries for any time $t \geq 0$. Let us discuss how the truncation errors affect the conservation of the divergence in the numerical scheme. The truncation in the representation of the fields $\mathbf{Z}^\sigma$ does not introduce any error in the evaluation of linear operators, such as space derivatives. On the contrary, aliasing errors arise in the calculation of nonlinear terms. Let us consider the numerical scheme (14)–(15) for the truncated quantities; taking the divergence of Eq. (14a) and using Eq. (15b) evaluated at the time t_n, we have

$$\left[1 - \frac{\theta \chi \Delta t}{2} \frac{\partial^2}{\partial x_k \partial x_k}\right]\left(\frac{\partial Z_i^{\sigma(*)}}{\partial x_i}\right) = \left[1 + \frac{\theta \chi \Delta t}{2} \frac{\partial^2}{\partial x_k \partial x_k}\right]\left(\frac{\partial Z_i^{\sigma(n)}}{\partial x_i}\right) - \theta \Delta t \left[Z_k^{-\sigma(n)} \frac{\partial}{\partial x_k}\right]\left(\frac{\partial Z_i^{\sigma(n)}}{\partial x_i}\right) + \varepsilon^\sigma, \tag{47}$$

where ε^σ is the aliasing error which arises in the calculation of the nonlinear terms. Even assuming that the truncated field $\mathbf{Z}^{\sigma(n)}$ at time $t = t_n$ is divergenceless, $\partial Z_i^{\sigma(n)}/\partial x_i = 0$, the aliasing error ε^σ acts as a source term for the field $\mathbf{Z}^{\sigma(*)}$ at time $t^* = t_n + \theta \Delta t$. A similar argument applied on Eqs. (15a) and (14b) shows that aliasing errors generate divergence in the truncated fields $\mathbf{Z}^{\sigma(n+1)}$. The time evolution of the divergence of $\mathbf{Z}^{\sigma(n)}$ then gives account of the effects of the cumulation of the aliasing errors in the pseudospectral numerical scheme. In Fig. 7 the quantities

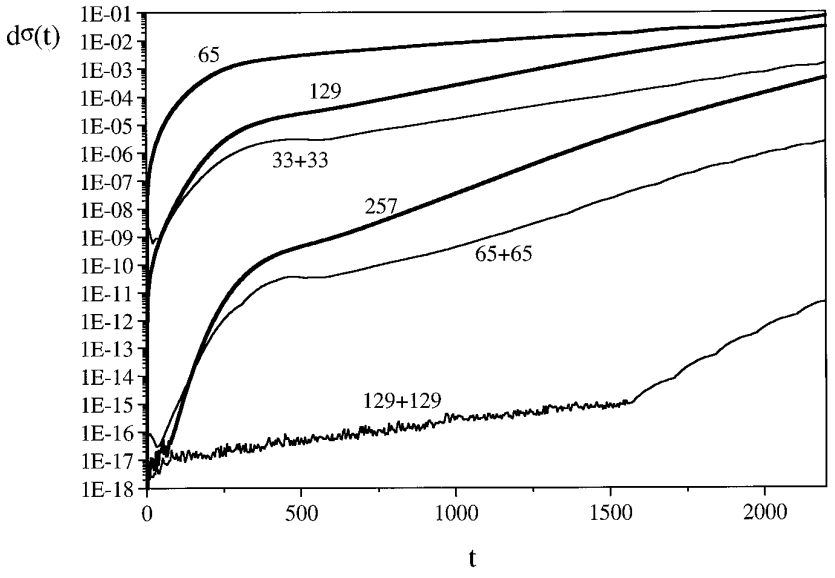

FIG. 7. The maximum divergences $d^+(t)$ and $d^-(t)$ are plotted as a function of the time. The total number of the employed Chebyshev polynomials is indicated. Thick lines refer to single-domain runs while thin lines refer to double-domain runs. For all the cases $d^+(t)$ and $d^-(t)$ are almost equal, so they appear superposed.

$$d^\sigma(t) = \max_{(x_i,y_j)\in D} \left| \frac{\partial Z_k^\sigma}{\partial x_k}(x_i, y_j, t) \right|, \quad \sigma = \pm, \tag{48}$$

are plotted as functions of the time, for the different runs performed using both the single-domain and the double-domain Chebyshev technique. The maximum is calculated over all the points in the spatial grid. For any run it has been found that, at any time t, $d^+(t)$ is very close to $d^-(t)$, so these quantities appear superposed. From Fig. 7 it can be seen that, using the same number of Chebyshev polynomials, much lower values of the maximum divergence are obtained with the double-domain technique than with the single-domain one. This is in accordance with the fact that the double-domain method in the problem under study gives origin to much lower truncation errors.

4. CONCLUSIONS

In this paper we have described the application of a pseudospectral Fourier–Chebyshev method to the solution of a problem in which a boundary layer forms, namely the development of the tearing instability in a plane sheet pinch. In the considered two-dimensional configuration the boundary layer is located along a straight line, where strong gradients in the direction perpendicular to such a line develop.

Our aim was to show that a better accuracy can be obtained using a double-domain Chebyshev technique rather than a standard single-domain technique, provided that the internal boundary between the two subdomains is located at the boundary-layer position, so that the strong gradients associated to it are close to the boundary of the Chebyshev mesh. The idea is based on the results by Solomonoff and Turkel [3], who studied the properties of pseudospectral Chebyshev expansions in cases when sharp gradients are present. These authors found that lower errors result when these gradients are localized near the boundary of the Chebyshev domain than when they are near the center.

On the basis of such results, we have split the computational domain in two subdomains, the internal boundary being along the line $x = 0$, where the boundary layer is located. In each subdomain a Chebyshev expansion has been performed with respect to the x-variable, i.e., in the direction of the strongest gradients, while a Fourier expansion has been used with respect to the y-variable. Standard collocation points have been used in the Chebyshev grid, since, as shown by Solomonoff and Turkel [3], in such a case the errors are lower than when a uniform mesh is used. The time scheme and the matching conditions at the internal boundary ensure that all the space derivatives are continuous across the internal boundary, up to the second order. Calculation of the numerical solution has been split in two by an influence matrix technique [9], which allows us to calculate the solution independently in each of the two subdomains. In this way two $(N + 1) \times (N + 1)$ linear systems are solved at each time step and for any Fourier harmonic, instead of one $2(N + 1) \times 2(N + 1)$ linear system.

The results obtained by the double-domain Chebyshev technique have been compared with those obtained by a single-domain technique. In this latter case, the boundary layer is located at the center of the Chebyshev mesh. The $m = 1$ Fourier harmonic corresponds to the unstable eigenmode in which the boundary layer forms. It has been found that the Chebyshev spectrum of this harmonic at a given time is much steeper when the double-domain method is used than in the single-domain case. This implies that if the same number of Chebyshev polynomials is used with the two techniques, much lower truncation errors are obtained with the double-domain method. For instance, considering the quantity Z_x, the truncation error obtained using 65 + 65 Chebyshev polynomials with the double-domain technique is smaller by a factor $\approx 10^6$ with respect to the truncation error obtained using 129 polynomials with the single-domain technique.

As a consequence, the double-domain Chebyshev technique allows us to obtain an accurate solution with a relatively low number of Chebyshev polynomials: in the considered case we found that using 33 + 33 polynomials a good accuracy is obtained in the numerical solution. On the contrary, using 65 polynomials with the single-domain technique a much worse result is obtained: strong oscillations are present in the space profiles of the solution and the time evolution is sensibly changed; in particular, the instability growth rate is lowered.

The pseudospectral method leads to aliasing errors in the evaluation of the nonlinear terms in the equations. For a given number of Chebyshev polynomials, such errors are lower if the sequence of the spectral coefficients of the solution goes to zero faster with increasing n. Since steeper Chebyshev spectra are obtained with the double-domain technique, smaller aliasing errors are obtained using such a technique. Actually, the effects of the aliasing errors observed in the Chebyshev spectrum of the solution are more relevant in the single-domain than in the double-domain cases. Another indicator of the aliasing errors is the divergence of the fields $\mathbf{Z}^\sigma$. In fact, this quantity must keep vanishing in the exact solution; on the contrary, in the numerical solution it grows as a consequence of aliasing errors. We found that the growth of the divergence is much slower using the double-domain than the single-domain technique. This is relevant, in particular, during the nonlinear stage of the instability, when the nonlinearities of the equations play a more important role in the time evolution.

APPENDIX

In this appendix we will show that

$$\|\hat{w}^{[\alpha]}(x, m)\|_\infty = 1, \quad m = 0, ..., M-1, \tag{A1}$$

where $\hat{w}^{[\alpha]}(x, m)$ are the correction solutions, and

$$\|g(x)\|_\infty = \sup\{g(x), x \in [-l, l]\}. \tag{A2}$$

Since $\hat{w}^{[R]}(x, m) = \hat{w}^{[L]}(-x, m)$, it is sufficient to prove (A1) only for $\hat{w}^{[R]}(x, m)$ in the interval $\{x \in [0, l]\}$. The solutions $\hat{w}^{[\alpha]}(x, m)$ fulfill the condition (20c),

$$\hat{w}^{[\alpha]}(0, m) = 1. \tag{A3}$$

Then, the relation (A1) is satisfied if the solutions $\hat{w}^{[R]}(x, m)$, which are continuous in the interval $[0, l]$, are also monotonically nonincreasing in the same interval. We will consider two cases:

(1) $\kappa(m) \neq 0$. In this case the general solution of Eq. (20a) is given by

$$\hat{w}^{[R]}(x, m) = c_1 e^{\kappa(m)x} + c_2 e^{-\kappa(m)x}, \tag{A4}$$

where c_1 and c_2 are constants which are determined by the boundary conditions. Let us indicate by x_e the value of x for which the derivative of the solution (A4) vanishes:

$$x_e = \frac{1}{2\,\kappa(m)} \lg \frac{c_2}{c_1}. \tag{A5}$$

If the boundary condition (16b) is given on the value of the solution

$$\hat{f}^{[R]}(l, m) = \hat{\beta}^{[R]}(m)$$

(this holds for the pressure, see Eq. (4)), then the boundary conditions (20b), (20c) for $\hat{w}^{[R]}(x, m)$ are

$$\begin{aligned} \hat{w}^{[R]}(l, m) &= 0, \\ \hat{w}^{[R]}(0, m) &= 1 \end{aligned} \tag{A6}$$

which give

$$c_1 = -\frac{e^{-l\kappa(m)}}{e^{l\kappa(m)} - e^{-l\kappa(m)}}, \quad c_2 = \frac{e^{l\kappa(m)}}{e^{l\kappa(m)} - e^{-l\kappa(m)}}.$$

Equation (A5) has no solution, since the ratio c_2/c_1 is negative, thus showing that $\hat{w}^{[R]}(x, m)$ is monotonic in $[0, l]$. Moreover, Eqs. (A6) indicate that $\hat{w}^{[R]}(x, m)$ is also decreasing in $[0, l]$.

If the boundary condition (16b) is given on the derivative of the solution

$$\frac{d\hat{f}^{[R]}}{dx}(l, m) = \hat{\beta}^{[R]}(m)$$

(this holds for $\mathbf{Z}^\sigma$; see Eq. (4)), then the boundary conditions (20b), (20c) for $\hat{w}^{[R]}(x, m)$ are

$$\frac{d\hat{w}^{[R]}}{dx}(l,m) = 0, \qquad \hat{w}^{[R]}(0,m) = 1 \tag{A7}$$

which give

$$c_1 = \frac{e^{-l\kappa(m)}}{e^{l\kappa(m)} + e^{-l\kappa(m)}}, \quad c_2 = \frac{e^{l\kappa(m)}}{e^{l\kappa(m)} + e^{-l\kappa(m)}}. \tag{A8}$$

Inserting these values in Eq. (A5) we find

$$x_e = l$$

which represents the upper limit of the space domain; this shows that $\hat{w}^{[R]}(x, m)$ is monotonic in $[0, l]$. Moreover, using the values (A8) in the expression (A4) it is found that

$$\hat{w}^{[R]}(l,m) = 1/\cosh\left[l\,\kappa(m)\right] \leq 1$$

which proves that $\hat{w}^{[R]}(x, m)$ is also decreasing in $[0, l]$.

(2) $\kappa(m) = 0$. In this case, which corresponds to the $m = 0$ Fourier harmonic of the pressure equation, the general solution of Eq. (20a) is given by a linear function

$$\hat{w}^{[R]}(x,0) = c_1 x + c_2, \tag{A9}$$

where c_1 and c_2 are constants which are determined by the boundary conditions. The solution (A9) is monotonically nonincreasing when $c_1 \leq 0$.

Actually, corresponding to the boundary conditions expressed by Eqs. (A6) we have

$$c_1 = -1/l, \quad c_2 = 1,$$

while, corresponding to the boundary conditions (A7) we have

$$c_1 = 0, \quad c_2 = 1.$$

In conclusion, in all the cases which we considered the solution $\hat{w}^{[R]}(x, m)$ is monotonically nonincreasing in the interval $[0, l]$ and this proves Eq. (A1).

ACKNOWLEDGMENTS

The author is grateful to A. Mangeney and V. Carbone for several helpful discussions on the subject of the paper. A particular thanks is due to P. Veltri for many suggestions and a critical reading of the manuscript. This work was partially supported by the Ministero della Università e della Ricerca Scientifica e Tecnologica on National Project Funds and by the Consiglio Nazionale delle Ricerche under Contract N.90.01253.CT02.

REFERENCES

1. D. Gottlieb and S. A. Orszag, *Numerical Analysis of Spectral Methods: Theory and Applications,* Regional Conference Series in Applied Mathematics, Vol. 26 (Soc. Indus. Appl. Math., Philadelphia, 1977).
2. S. Bonazzola and J.-A. Marck, *J. Comput. Phys.* **97,** 535 (1991).
3. A. Solomonoff and E. Turkel, *J. Comput. Phys.* **81,** 239 (1989).
4. H. P. Furth, J. Killeen, and M. N. Rosenbluth, *Phys. Fluids* **6,** 459 (1963).
5. T. D. Taylor, R. S. Hirsh, and M. M. Nadworny, *Comput. & Fluids* **12,** 1 (1984).
6. D. S. Harned and W. Kerner, *J. Comput. Phys.* **60,** 62 (1985).
7. D. S. Harned and D. D. Schnack, *J. Comput. Phys.* **65,** 57 (1986).
8. S. A. Orszag, *J. Comput. Phys.* **37,** 70 (1980).
9. C. Canuto, M. Y. Hussaini, A. Quarteroni, and T. A. Zang, *Spectral Methods in Fluid Dynamics* (Springer-Verlag, New York, 1988).
10. F. Porcelli, *Phys. Fluids* **30,** 1734 (1987).
11. G. Einaudi and F. Rubini, *Phys. Fluids B* **1,** 2224 (1989).
12. F. Malara, P. Veltri, and V. Carbone, *Phys. Fluids B* **4,** 3070 (1992).
13. S. A. Orszag, *J. Fluid Mech.* **49,** 75 (1971).
14. S. A. Orszag, *Stud. Appl. Math.* **51,** 253 (1972).